



HAL
open science

3D rGO aerogel with a superior electrochemical performance for K -Ion battery

Liyuan Liu, Jean-Yves Chane-Ching, Zifeng Lin, Hui Shao, Pierre-Louis Taberna, Patrice Simon

► **To cite this version:**

Liyuan Liu, Jean-Yves Chane-Ching, Zifeng Lin, Hui Shao, Pierre-Louis Taberna, et al.. 3D rGO aerogel with a superior electrochemical performance for K -Ion battery. *Energy Storage Materials*, 2019, 19, pp.306-313. 10.1016/j.ensm.2019.03.013 . hal-02362049

HAL Id: hal-02362049

<https://hal.science/hal-02362049>

Submitted on 13 Nov 2019

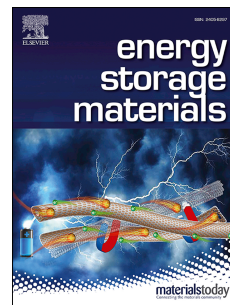
HAL is a multi-disciplinary open access archive for the deposit and dissemination of scientific research documents, whether they are published or not. The documents may come from teaching and research institutions in France or abroad, or from public or private research centers.

L'archive ouverte pluridisciplinaire **HAL**, est destinée au dépôt et à la diffusion de documents scientifiques de niveau recherche, publiés ou non, émanant des établissements d'enseignement et de recherche français ou étrangers, des laboratoires publics ou privés.

Accepted Manuscript

3D rGO aerogel with a superior electrochemical performance for K – Ion battery

Liyuan Liu, Zifeng Lin, Jean-Yves Chane-Ching, Hui Shao, Pierre-Louis Taberna, Patrice Simon



PII: S2405-8297(18)31479-X

DOI: <https://doi.org/10.1016/j.ensm.2019.03.013>

Reference: ENSM 677

To appear in: *Energy Storage Materials*

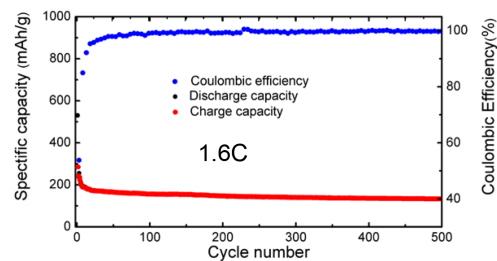
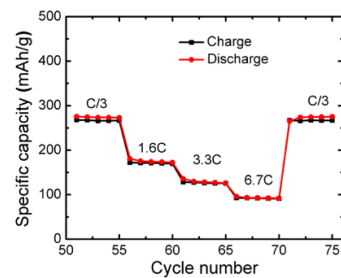
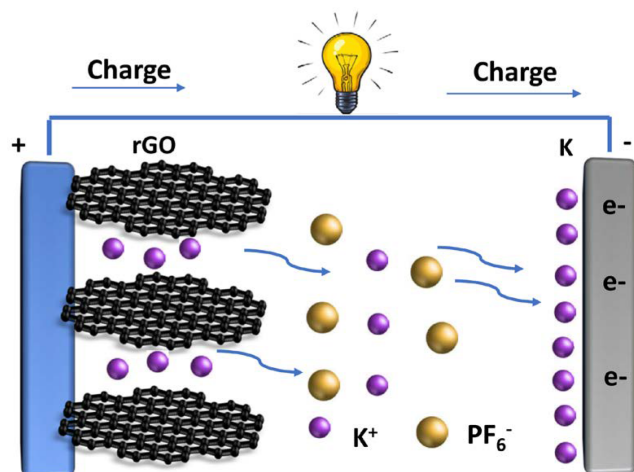
Received Date: 13 December 2018

Revised Date: 13 February 2019

Accepted Date: 15 March 2019

Please cite this article as: L. Liu, Z. Lin, J.-Y. Chane-Ching, H. Shao, P.-L. Taberna, P. Simon, 3D rGO aerogel with a superior electrochemical performance for K – Ion battery, *Energy Storage Materials* (2019), doi: <https://doi.org/10.1016/j.ensm.2019.03.013>.

This is a PDF file of an unedited manuscript that has been accepted for publication. As a service to our customers we are providing this early version of the manuscript. The manuscript will undergo copyediting, typesetting, and review of the resulting proof before it is published in its final form. Please note that during the production process errors may be discovered which could affect the content, and all legal disclaimers that apply to the journal pertain.



**3D rGO aerogel with a superior electrochemical performance for
K – ion battery**

ACCEPTED MANUSCRIPT

Abstract

As one possible alternative metal to lithium in ion batteries, potassium has recently attracted considerable attention as a result of its geochemical abundance and low cost. In this work, a detailed study of the electrochemical properties of potassium ion storage was performed using reduced graphene oxide (rGO) aerogel as a negative electrode material. The influence of the nature of the electrolyte and the drying methods used were investigated in order to optimize the electrochemical performance of freeze-dried rGO in potassium-ion batteries (PIBs). Electrochemical impedance spectroscopy (EIS) were used to assess the performance of our rGO material in PIBs. Used as the negative electrode, freeze-dried rGO can deliver a high capacity of 267 mAh/g at C/3 rate together with 78% capacity retention during 100 cycles, combined with high rate capability (92 mAh/g at 6.7 C). This set of results makes rGO aerogel a promising electrode material for PIBs.

Keywords

Reduced graphene oxide, rGO aerogel, K-ion battery, Anode materials.

1. Introduction

With the booming development of renewable energy sources, the need for advanced large-scale electrochemical energy storage devices is becoming imminent. Although great efforts have been devoted since the 1990s to improve Lithium-Ion Batteries (LIBs) performance to fit with a wide range of applications, the development of alternative energy storage devices must not be stopped considering the scarcity of Lithium resources and uneven distribution [1]. In this context, rapid progresses have been recently achieved to develop Na-Ion Batteries (NIBs) [2], since sodium is a less expensive and relatively abundant element [3]. Thanks to great research efforts, many layered metal oxides [4] and polyanionic compounds [5]

demonstrated great capacity, [6] cyclability [7] and multi-electron transfer [8,9] as cathode materials for NIBs, which make NIBs become a potential alternative to LIBs for some applications where energy density is not the main requirement [10]. However, the standard electrode potential of Na/Na⁺ (-2.71 V vs. standard hydrogen electrode) is 330 mV higher than that of Li/Li⁺ (-3.04 V vs. standard hydrogen electrode), thus resulting in a lower output working voltage and lower energy density compared to LIBs.

Recently, Potassium-Ion Batteries (PIBs) have focused a lot of attention as a new energy storage system since they offer several key advantages versus LIBs. First, the abundance of K resources is similar to Na [1] resulting in low cost of potassium versus lithium (~1000 USD per ton of Lithium carbonate compared to ~6500 USD per ton of potassium carbonate [1]). Also, the standard electrode potential of K/K⁺ (-2.93 V vs. standard hydrogen electrode) is lower than that of Na/Na⁺ (-2.71 V vs. standard hydrogen electrode), allowing PIBs to operate at higher voltage, close to that of LIB, resulting in improved energy density versus NIBs [11]. Then, according to the report of Okoshi et al [12], K electrolytes exhibit higher conductivity than Li and Na electrolytes. (4) Additionally, in contrast to LIBs, aluminum foil can replace the costly copper foil as negative current collector since there is no KxAl alloy formation reported [13]. Last but not least, the most significant advantage of PIBs technology over NIBs technology is that graphite ne used as negative electrode material since it can accommodate reversible K-ion de/intercalation [11]. In contrast to sodium, potassium can be intercalated reversibly into graphite to form KC₈, leading to a theoretical capacity of 280 mAh/g [14,15]. Aside from graphite, many other materials have proven recently to be promising for PIBs such as Soft carbon [15], Prussian blue [16,17], Hard–Soft composite carbon [18], N-doped carbon [19], Sn₃P₄ [20], and MoS₂ [21,22]. But there is still room for improvement since one of the major flaws is the poor transport kinetic of K-ions, principally due to its large size (0.138 nm), with respect to Na (0.102 nm) or Li ions (0.076 nm).

Here, we report about the use of 3D reduced Graphene Oxide (rGO) aerogel as anode material for PIBs. Graphene has been recently proposed by *Luo et al.* [23] as an anode material in PIBs. *Luo et al.* reported that rGO had both a poor rate capability and cycling stability due to low K^+ ionic conductivity [23]. Since then, numerous efforts have been made to overcome such limitations for instance by tuning the electronic structure and expanding the interlayer spacing of graphene by doping with various heteroatoms [24-26]. Doing so, it has been reported that the K-ion storage capacity and cycling stability could be improved. Our approach here consists in enhancing the ionic transport within rGO material by (1) tweaking the morphology of the rGO and (2) selecting the suitable electrolyte to achieve improved K-ion storage capacity, good rate capability, and long cycling life.

2. Experimental

2.1. Preparation of Reduced Graphene Oxide

Natural graphite (KS44 graphite, purchased from IMERYS Graphite & Carbon Corporation) was used as the precursor. Graphene oxide (GO) was prepared by the modified Hummers' method. In a typical procedure, 120 mL of H_2SO_4 (95 wt%) and 13 mL of H_3PO_4 (85 wt%) were added into a flask and stirred for 10 minutes to achieve a homogeneous solution. After addition of 1.0 g flake graphite powder, 6.0 g of $KMnO_4$ was slowly added into the flask with vigorous stirring under the protection of an ice-water bath. The reaction was held at 50 °C with continuous stirring for 12 hours. After addition of 1 mL of 30 wt% H_2O_2 , the color of the solution turned from dark green to bright yellow (Figure S1a). The obtained graphene oxide was washed by distilled water, 30% HCl and then in absolute ethanol as a sequence, until a pH of 8.5 was reached. Ultrasonic treatment was used to further exfoliate the GO nanosheets. Three different routes were selected to dry the graphene oxide: (1) vacuum freeze-drying for 4 days, (2) oven drying at 60 °C for 12 hours, (3) oven drying at 100 °C for 30 minutes. To reduce graphene oxide, the as-prepared GO aerogel was heated for 10 hours at 350 °C at a heating rate of 5 °C/min in Ar mixed atmosphere followed by ultrasonic treatment for 1 h to further exfoliate the graphene nanosheets or for two

years at 80 °C inside a vacuum oven.

2.2. Physical characterizations

X-ray diffraction (XRD) data was collected by a D4 ENDEAVOR X-ray diffractometer (Bruker, Germany) equipped with $\text{CuK}\alpha$ radiation ($\lambda = 0.154$ nm). The morphology of the rGO was observed with a Scanning Electron Microscope (SEM) JSM 7100F (JEOL, Japan). Nitrogen adsorption-desorption isotherms were measured at 77K using a Micromeritics ASAP 2020. The Brunauer–Emmett–Teller (BET) equation was used to calculate the specific surface area (SSA), from the linear plot in the relative pressure range (P/P_0) 0.01-0.35. The pore size distribution (PSD) was determined by non-local density functional theory (NLDFT) standard model with SAIEUS software.

2.3. Electrochemical measurements

Two-electrode Swagelok[®] cells were assembled in an argon-filled glove box (**moisture < 0.1 ppm, oxygen < 0.1 ppm**) to perform electrochemical measurements. rGO aerogel has been pressed under 10-ton pressure using hydraulic press machine first and then cut to get the desired shape with a cutter (diameter: 9 mm). After that, rGO aerogel was directly used as the working electrode to assemble standard half-cells with a K metal (99.5%, Sigma-Aldrich) as counter and reference electrode. Depending on the cell, the active mass loading was between 0.7 and 1 mg/cm². Aluminum foils were used as current collectors, while two layers of 260 μm -thick porous borosilicate glass fibers (Whatman GF/B) were used as the separator.

All electrochemical characterizations were done at room temperature using a multichannel VMP3 electrochemical working station (Biologic, S.A.). Galvanostatic cycling was carried out within a potential range from 0.01 to 3V vs. K/K⁺.

Three different electrolytes were selected to optimize the electrochemical performance of PIBs, they are (1) 0.7 M KPF_6 (99.5%, Sigma-Aldrich) dissolved in

ethylene carbonate/propylene carbonate solvent (EC:PC = 1:1 by volume), (2) 0.7 M KPF₆ dissolved in ethylene carbonate/diethyl carbonate (EC:DEC = 1:1 by volume), and (3) 0.7 M KPF₆ dissolved in PC. **The water content in all as-prepared electrolytes was measured by Karl-Fisher titration and found to be lower than 50 ppm in all cases.**

3. Results and discussion

3.1. Characterization of morphology and structure

The composition and structure of the samples were first analyzed by XRD. As expected, two typical peaks can be observed in pristine graphite (Fig. 1a), with (002) peak around 26.0° and (100) peak around 43.0°. After oxidation, the (100) characteristic diffraction peak is shifted from 26.0° to 9.5° due to the increased interlayer spacing. The layer spacing could be calculated using Bragg's law (equation 1):

$$d = \lambda / [2 \sin (\theta)] \quad (1)$$

where $\lambda = 0.154$ nm is the wavelength of the X-ray beam, d is the layer spacing, θ is the diffraction angle. According to the above equation, the interlayer spacing has been increased from 0.335 nm to 0.913 nm, which indicates the successful preparation of GO from graphite.

SEM image shown in Fig. 1b reveals that the freeze-dried rGO consists of the layered structure of ultrathin nanosheets. The transparency of the sheets evidences small thickness and limited restacking of the 2D structures. The open architecture of the freeze-dried rGO and the wide space between the rGO layers should be favorable for K⁺ ion intercalation. For comparison, the morphology of rGO samples dried at 60 °C and 100 °C are also shown in Figure S2. Differently from transparent silk-like nanosheets of freeze-dried rGO (Fig. 1b), an important restacking was observed for rGO dried at 100 °C (Fig. S2a), resulting in thicker multi-layered 2D structures. Such a restacking of rGO layers decreases the accessible surface area of the sample.

Gas sorption experiments using N_2 at 77K were conducted to measure the specific surface area, porous volume, and pore size distribution. The presence of a hysteresis loop at $P/P_0 = 0.5-1.0$ in the type-IV isotherm shown in Fig. 1c suggested the presence of mesopores. The BET surface area was found to be $219 \text{ m}^2/\text{g}$, and the total porous volume was $0.35 \text{ cm}^3/\text{g}$. Fig. 1d shows the pore size distribution of the **freeze-dried** rGO sample obtained from the 2D-NLDFT model. The mesoporous volume was measured at $0.28 \text{ cm}^3/\text{g}$ that is 82% of the total porous volume, in agreement with the type IV isotherm. **Differently, The SSA of the freeze dried sample ($219 \text{ m}^2/\text{g}$) was 2.5 times larger than that of the 60°C dried sample ($86 \text{ m}^2/\text{g}$), resulting in lower accessible surface for K ion intercalation for the the rGO sample dried at 60°C (see Figure S3a and S3b). The porous volume was also divided by ~ 5 times when moving from freeze-dried to 60°C dried sample. The hierarchical morphology and high surface area obtained for the freeze-dried rGO sample should favor the surface accessibility of K^+ .**

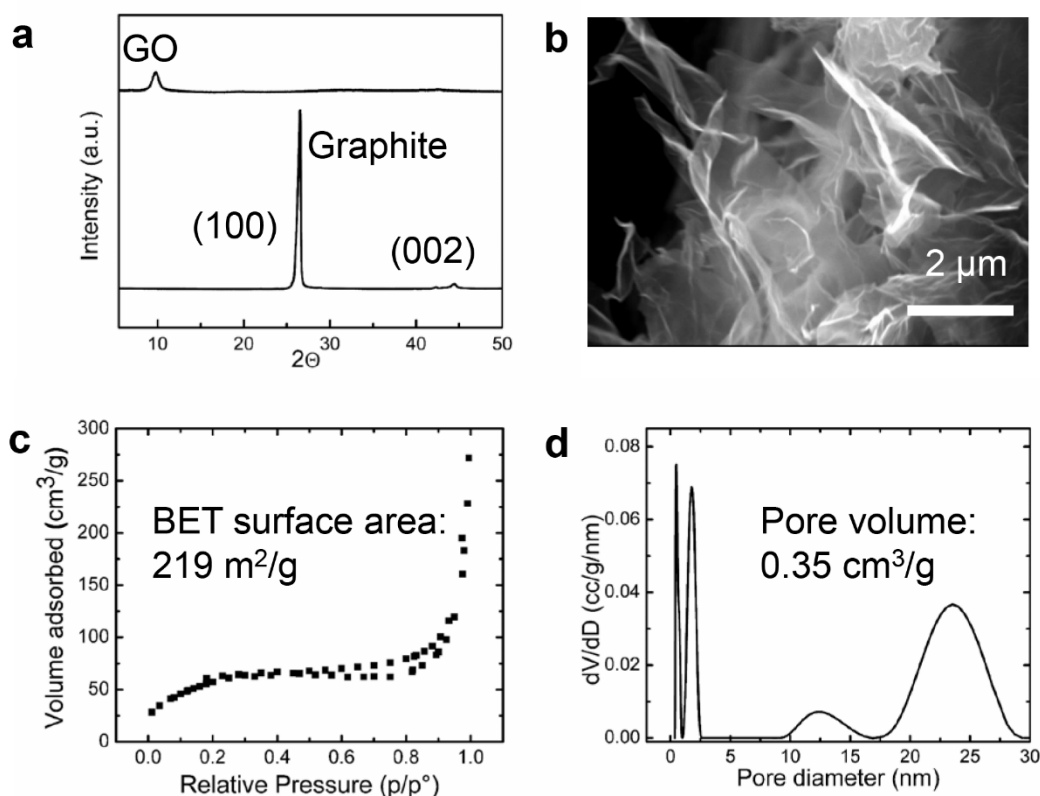


Fig. 1. (a) XRD patterns of graphite and GO, (b) SEM graph of freeze-dried rGO sheets, (c) Nitrogen-adsorption isotherms **of freeze-dried rGO**, (d) Desorption pore-size distribution and pore volume **of freeze-dried rGO material**.

3.2. Electrochemical performance

As well known, the morphology of 2D materials and the electrolyte composition play a significant role on the electrochemical performance [28]. In this work, various drying methods for preparing the rGO electrode and different electrolytes have been tested in rGO aerogel / K-metal half-cells to explore the effects of morphology and electrolyte composition on the electrochemical performance.

3.2.1. Comparison of different electrolytes and drying methods

It is well known that the electrolyte has an important impact on the formation of a stable solid SEI layer for Li- and Na-ion battery negative electrode [28-30].

Fig. 2 shows the comparison of the electrochemical performance of our freeze-dried rGO anode in three different electrolytes containing 0.7M KPF₆ salt dissolved in a) EC:PC, b) EC:DEC and c) PC solvents. The K⁺ insertion in rGO electrodes occurs at the potential below 1.2 V vs. K⁺/K in all the selected electrolytes, in agreement with previous report [26]. Demonstrably difference can be seen regarding the first discharged capacity and the coulombic efficiency in the various electrolytes. The theoretical capacity of a carbon electrode for K⁺ intercalation being 280 mAh/g (considering KC₈ as the fully reduced phase), the measured discharged capacity in the range of 900 to 2400 mAh/g is linked with SEI layer formation as well as probably irreversible reduction of surface groups present at rGO surface [26]. Higher initial coulombic efficiency (44%) was obtained in EC:PC electrolyte in comparison with EC:DEC (26%), which is similar to what has been observed in graphite for KIB [31]. However, very low initial coulombic efficiency (6%) (see Fig. 3c) and significant capacity decay was observed using pure PC as solvent in the electrolyte, this is similar to what is observed with hard carbon in SIB anode which has been attributed to the

continual decomposition of PC and growth of an SEI film [28]. EC is favored as a co-solvent since it results in the formation of a protective-layer SEI, which was verified not only in LIBs but also in SIBs [28-30]. However, pure EC is not suitable as a solvent at ambient temperature because of its high melting point (36 °C) [30]. Moreover, stable efficiency corresponding to stable SEI layer formation was achieved after ~ 10 cycles in EC:PC electrolyte, while much lower coulombic efficiency of first 10 cycles was observed in EC:DEC (Fig. 2d). Besides, better capacity retention ability has been observed with 0.7M KPF₆ in EC:PC electrolyte compared to 0.7M KPF₆ in EC:DEC electrolyte (Fig. S4). Those results are consistent with lower stability of linear versus cyclic carbonates **at low voltage**, as it has been observed for Na-ion batteries [28]. **Indeed, Ponrouch et al. measured thermal and electrochemical stability of various electrolytes containing diverse solvent mixtures (cyclic, acyclic carbonates, glymes) and Na based salts (F-based or perchlorate anions), for sodium ion battery applications [28]. Based on electrochemical impedance spectroscopy and CV measurements, wider electrochemical stability window was measured for EC:PC mixture among numerous solvents [28]; this was mainly attributed to the improved electrochemical stability of cyclic carbonates versus linear ones. Moreover, differential scanning calorimetry measurements showed a single exothermic peak around 250°C for EC:PC mixture, resulting in the best thermal stability amongst all the solvent combinations tested [28]. In summary, our results with rGO electrode confirm that EC:PC based electrolyte has important advantages in terms of safety and wider electrochemical potential window.** As a result, 0.7M KPF₆ in EC:PC electrolyte was selected for studying the power performance and cycling stability of the rGO electrode.

The drying method used to prepare rGO materials has also a significant impact on electrochemical performance. Differently from freeze-dried rGO, Fig. S5 shows that rGO dried at 100°C for 30 minutes is not electrochemically active for K⁺ intercalation, while a rGO dried at 60°C (Fig. S6) exhibits limited electrochemical activity compared with freeze-dried rGO. Such a behavior can be explained by the restacking of rGO layers for non-freeze-dried samples, resulting in limited surface accessibility for K-ion insertion. This restacking may explain the poor performance of

rGO electrode for K-ion battery, as recently reported by *Xie et al.* [22] and *Luo et al.* [23]. It is well known that the freeze-drying method is a simple and efficient way to retain the microstructure and specific surface area of the treated samples during the drying process. The excellent rate performance and cycling stability thus can be achieved since the freeze-drying process plays an important role in prevention of the restacking of graphene sheets [27].

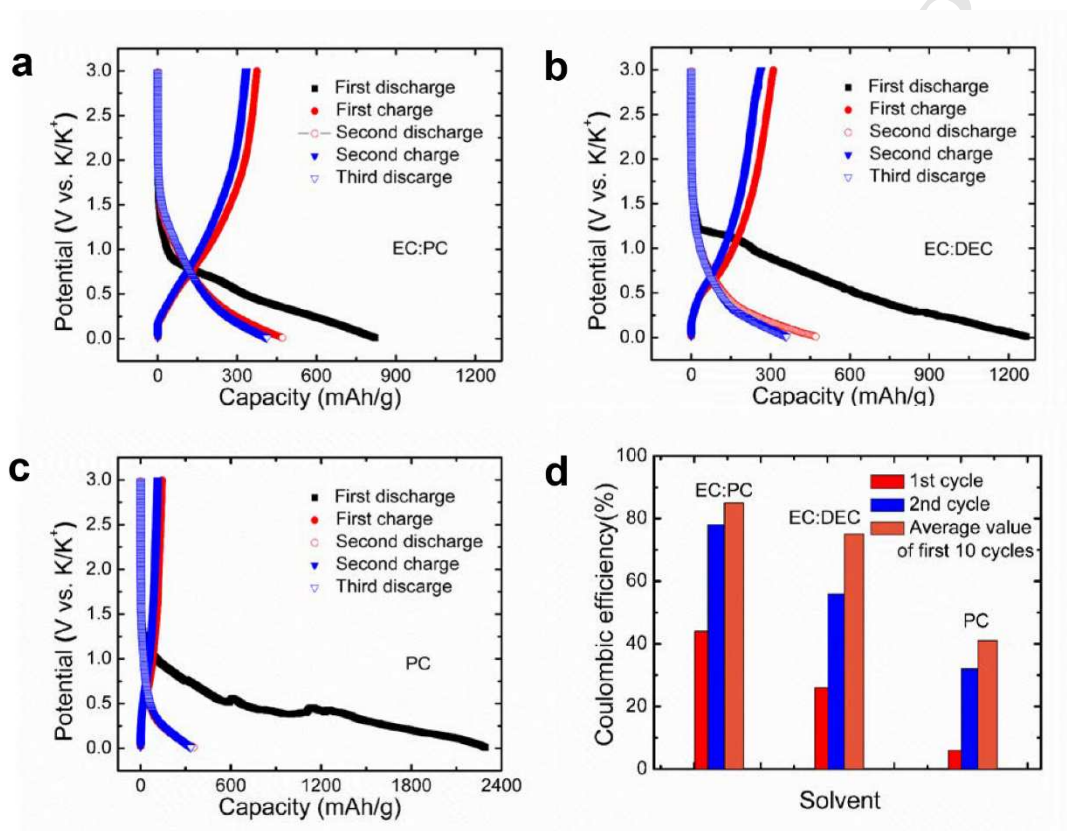


Fig. 2. Comparison of initial three cycles of charge-discharge curves of rGO electrode at C/3 in (a) 0.7M KPF₆:EC:PC, (b) 0.7M KPF₆:EC:DEC and (c) 0.7M KPF₆:PC electrolytes. (d) Comparison of the coulombic efficiency of rGO electrode at C/3 in the three electrolytes.

The derivative dQ/dV plots for the first three charge-discharge cycles are shown in Fig. 3a. K⁺ insertion into rGO during the first reduction (discharge) process results in

the appearance of three cathodic peaks. The electrochemical signature is consistent with the results previously reported by *Ju et al.* [26]. The first peak at about 0.71 V vs. K^+/K corresponds to the decomposition of the electrolyte and the associated formation of a stable solid SEI layer [26] as well as the starting of the intercalation of K ions into rGO electrode. The second cathodic peak (centered around 0.32 V) is related to further intercalation of K^+ into rGO until the potential of 0.02 V which corresponds to the third cathodic peak (Fig. 3a). The three observed anodic peaks located at 0.05 V, 0.31 V, and 0.66 V during the reverse scan correspond to K^+ deintercalation reaction.

Fig. 3b and c shows the electrochemical performance of freeze-dried rGO electrode in 0.7M KPF_6 in EC:PC electrolyte at various current densities. The electrode capacity was stable at about 267 mAh/g at C/3 rate which is close to its theoretical capacity. Fig. 3b shows that a capacity of about 92 mAh/g can be still achieved at a high current rate of 6.7C, which evidences high power capability for our freeze-dried rGO electrode compared to the literature [23]. Cycling stability was tested at the constant current rate of C/3 (see Fig. 3d). It reveals that the capacity can still retain about 230 mAh/g over 100 cycles, gives a good capacity retention of 78%. However, the coulombic efficiency was close to 95% during the first 10 cycles, before reaching 98% after 15 cycles. Such initial coulombic efficiency can be attributed to the presence of oxygen surface functional groups remaining on the rGO surface. A longer reduction treatment time could improve the coulombic efficiency. The electrochemical capability at large current density (1.6 C) was also tested, which exhibits high cycling stability (Fig. 3e). Even after 500 cycles, a charge/discharge capacity of 125 mAh/g was still achieved.

To the best of our knowledge, the high K-ion insertion capacity, rate capability and capacity retention upon cycling in 0.7M KPF_6 :EC:PC electrolyte for the present

freeze-dried rGO aerogel compares positively with most of the other previously reported carbon-based anodes used in PIB (Table S1). Additionally, the simple synthesis route and the limited synthesis temperature (350°C) used to prepare our rGO makes it competitive versus all the carbon-based materials used as negative electrode in K-ion batteries listed in Table S1. For example, *Ma et al.* reports about a phosphorous doped-rGO material with high capacity (160 mAh/g at 2 A/g) as well as stable cyclability over 600 cycles with a coulombic efficiency of 35% at the first cycle [25]. However, this materials is based on P-doped graphene, with a complicated synthesis process which need high temperature (900°C) treatment [25]. *Jian et al.* reported another kind of active material, Hard–Soft composite carbon with a good capacity of 150 mAh/g at 5C as well as a stable cycling over 200 cycles, whose synthesis is also achieved at high temperature (900°C) [18]. Although the rGO aerogel can be easily prepared at lower cost thanks to simple synthesis process, its electrochemical performance (120 mAh/g after 500 cycles) are close to those hard and soft carbon materials [15,18] and heteroatom doped graphene [24-26], making freeze-dried rGO an interesting anode for K-ion battery applications.

Such achieved performances are in-line with the expected enhancement of K^+ diffusion thanks to microstructuration obtained by freeze-drying of rGO. Nevertheless, to confirm this aspect further analysis have been done by Electrochemical Impedance Spectroscopy.

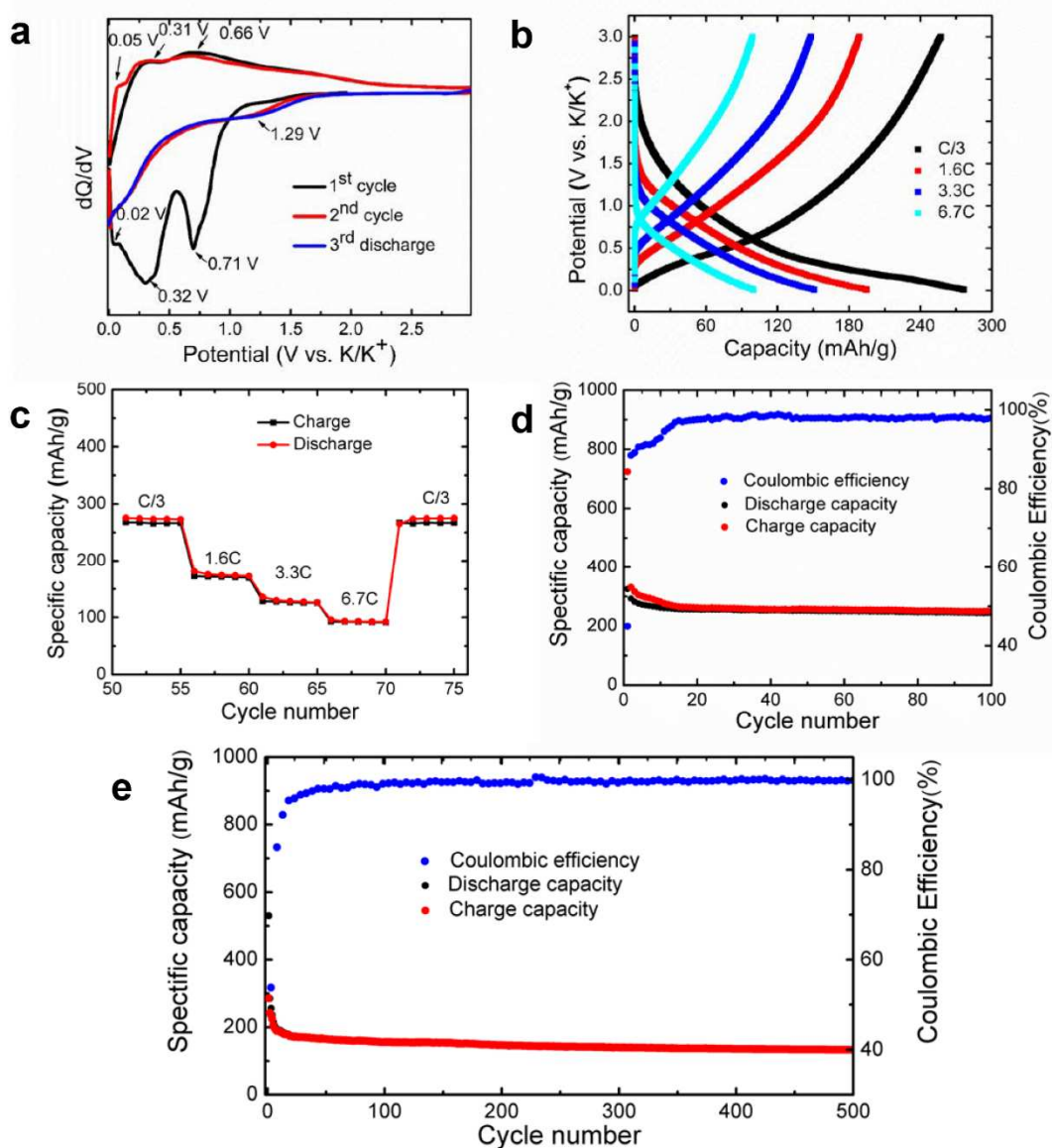


Fig. 3. Electrochemical performance of rGO aerogel in 0.7M KPF₆:EC:PC electrolyte: (a) differential capacity plots (dQ/dV) corresponding to the voltage profiles in Fig. 2a; (b) discharge-charge curves of rGO at various C-rates; (c) cycling capability after 50 cycles at C/3; (d) charge and discharge capacity retention at long-cycle stability test at C/3. (e) charge and discharge capacity retention at long-cycle stability test at 1.6C.

3.2.2. Reaction kinetics

In-depth investigations of the K-ion storage mechanism was achieved using cyclic voltammetry at different scan rates. Based on the relationship between the peak current (i) and scan rate (v) [32]

$$i = av^b \quad (2)$$

the b-value can be determined by plotting the (i) vs. (v) curves in log scale, calculated from CV curves recorded at various scan rates (see Fig. 4a). A b-value of 1 indicates that the charge storage is totally dominated by a surface (non-diffusion limited) process, whereas 0.5 evidences a bulk (diffusion-limited) process, controlled by the K ion solid-state diffusion in the rGO material. b value was found to be 0.72 (see Fig. 4b), which indicates that both contributions (surface and bulk) are present. *Dunn and et al.* [32] proposed a method based on the deconvolution of the current into surface (changing with v) and diffusion-limited contributions (changing with $v^{1/2}$), at each potential, leading to equation (3):

$$i(v) = k_1v + k_2v^{1/2} \quad (3)$$

where k_1 and k_2 are two constants, i the current (mA) and v the potential scan rate (V/s). Figs. 4c shows the contributions of the surface (non-diffusion limited) and bulk (diffusion-limited) charge processes at a scan rate of 1 mV/s, calculated from equation (3). Even at such low scan rate of 1 mV/s, those results show that the fast surface process plays a significant role in the charge storage, thus supporting the high rate performance of the freeze-dried rGO electrode. The capacitive charge contributions at various scan rates from 0.1 to 10 mV/s are presented in Fig. 4d. As expected, the fast surface charge contribution get higher as the scan rates increase and finally reach a maximum values of 68% at a potential scan rate of 10 mV/s.

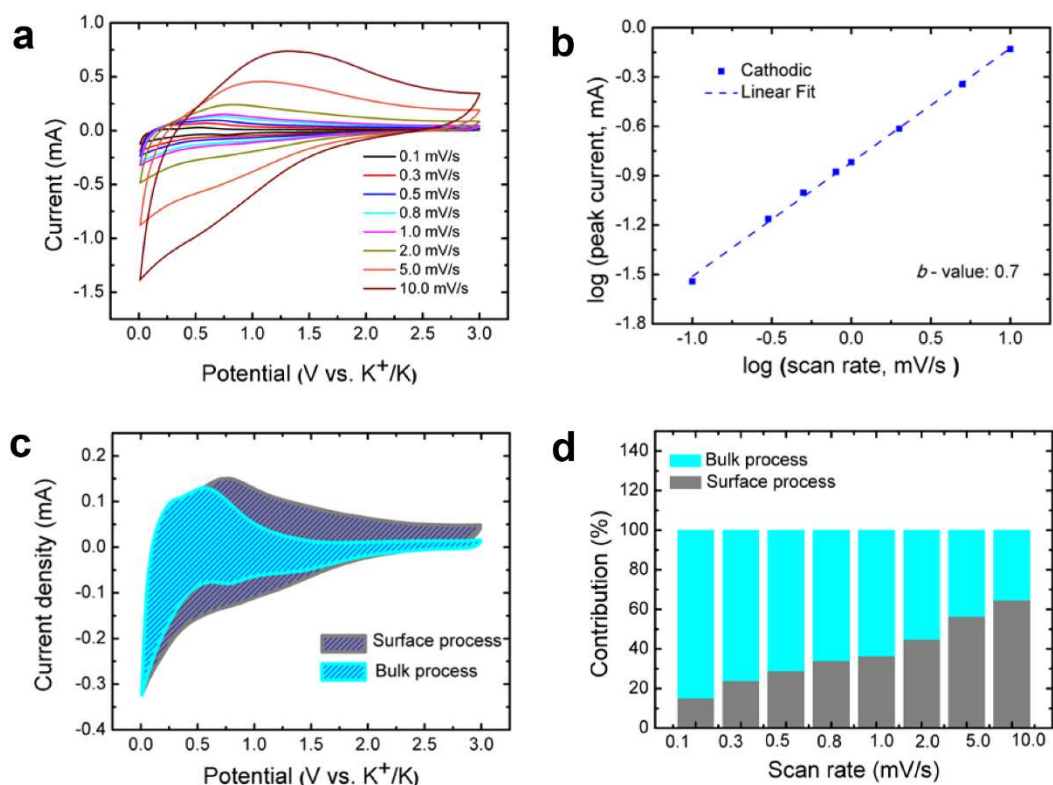


Fig. 4. (a) CV curves recorded at various potential scan rates from 0.1 to 10 mV/s; (b) Determination of the b- coefficient using the relationship between peak current and scan rate; (c) Separation of the surface (non-diffusion limited) and bulk (diffusion-limited) processes of charge storage at 1.0 mV/s; (d) Surface and bulk current contributions to the total charge versus the scan rates from 0.1 to 10 mV/s.

Electrochemical impedance spectroscopy (EIS) measurements were achieved at different potentials during the first K ion intercalation cycle to understand the reaction process thoroughly. A conventional three-electrode setup (Fig. S7) was used, with rGO (containing 20% carbon black) as a working electrode and K metal as both counter and reference electrodes. As shown in Fig. 5a, at OCV, the impedance shows a fast increase of the imaginary part at low frequency, which is typical of a blocking-type electrode behavior in the absence of a charge transfer reaction [26]. When the potential is decreased, another semicircle starts growing in the middle frequency range, which can be associated to the presence of the SEI film together with the charge transfer process corresponding to the first steps of K ion intercalation reaction,

in agreement with the results presented in Fig. 3a. With a further decrease of the potential down to 0.4 V and 0.1 V, the charge transfer resistance decreases due to the larger polarization potential. During charge (oxidation) from 0.1V to 0.6 V, the growth of the semi-circle diameter is consistent with the increase of the charge transfer resistance of K-ion de-intercalation reaction (Fig. 5b). At low frequency, the rise in impedance follows a Warburg-type behavior linked to diffusion of K ion inside rGO electrode in agreement with ref. 26.

The similar impedance signatures between the 1st and 5th cycle shown in Fig. 5b and 5d evidence the stabilization of the electrochemical behavior (charge transfer and SEI film formation processes). Moreover, the smaller impedance observed during reduction (Fig. 5c) versus oxidation (Fig. 5d) mainly originates from the decrease of the charge transfer resistance, that is to say, faster reaction kinetics is observed upon reduction.

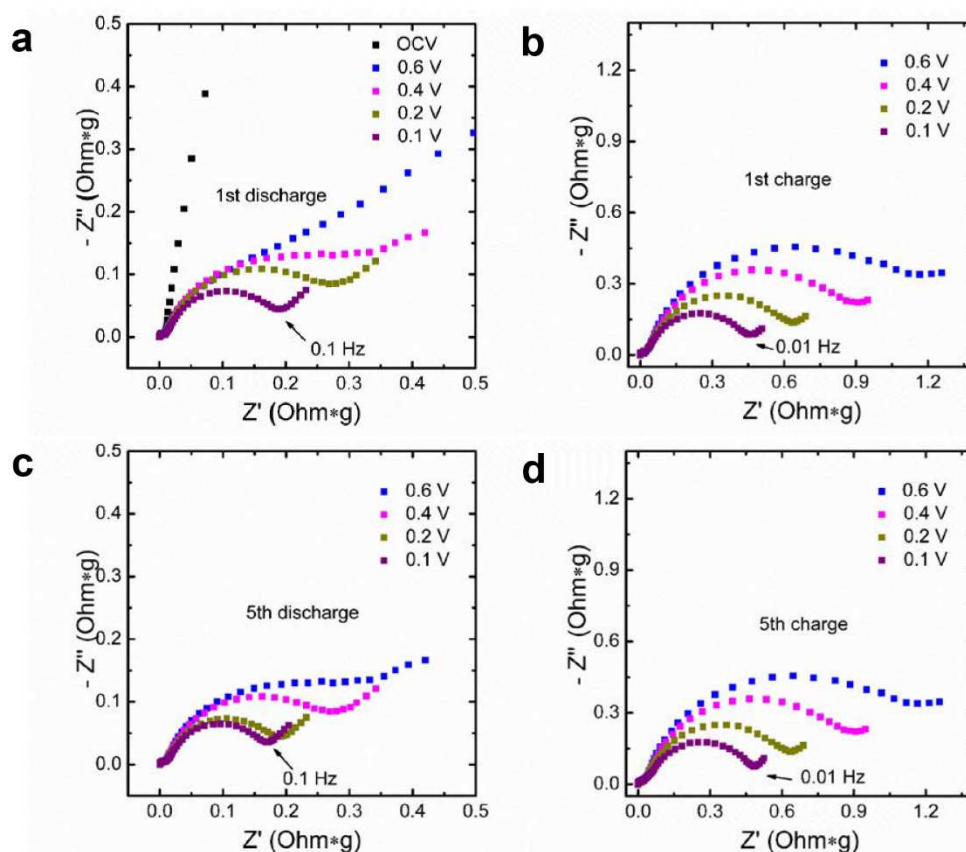


Fig. 5. EIS analysis at different potentials using a three-electrode set-up during: (a) the first discharge (reduction) cycle; (b) the first charge (oxidation) cycle; (c) the fifth discharge; (d) the fifth charge cycle, respectively.

The diffusion coefficient of K ion into the rGO electrode was calculated from the impedance measurements shown in Fig. 5c and 5d. Fig. 6a shows an example of the apparent diffusion coefficient of K ion into rGO electrode calculated from the low frequency region of the impedance plot, using equation 3:

$$D = \frac{1}{2} \left(\frac{RT}{AC\sigma z^2 F^2} \right)^2 \quad (3)$$

where A is the surface area of the electrode, z is the valence of the ion, F is the Faraday constant, C is the concentration of potassium ion in rGO electrode, R is the gas constant, T is the room temperature in our experiment, σ is the slope of the line $Z' \sim \omega^{-1/2}$ which can be obtained from the line of $Z' \sim \omega^{-1/2}$ (shown in Fig. 6a). Figure 6b shows the apparent diffusion coefficient change of K ion with electrode potential during both intercalation (reduction) and de-intercalation (oxidation) processes. The K-ion diffusion coefficient is about 10^{-9} cm²/s at 0.1V, which is similar to the results of K-ion solid diffusion coefficient calculated for N- doped rGO [26] and higher than that of graphite anode calculated by Galvanostatic Intermittent Titration Technique [31]. This high diffusion coefficient of the K-ions provides good rate capability, as a result of the open structure of our present freeze-dried rGO material.

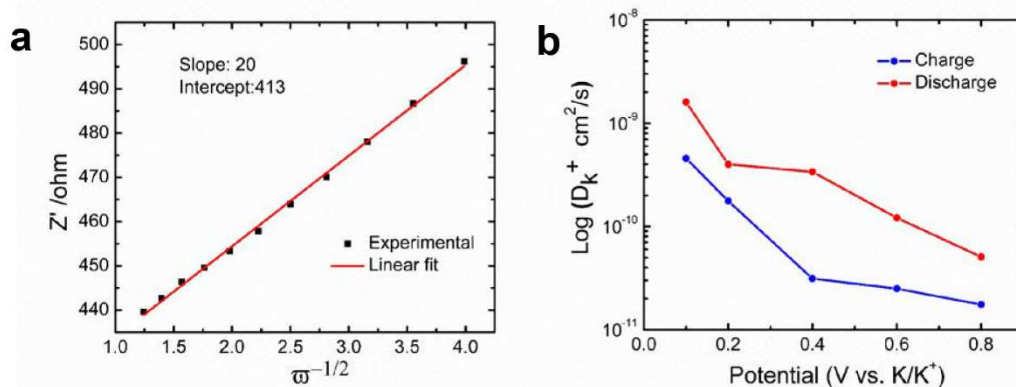


Fig. 6. (a) $Z'' \sim \omega^{-1/2}$ line in the low-frequency region of the third discharge cycle at 0.1 V; (b) Diffusion coefficients calculated from the impedance results.

4. Conclusions

Reduced graphene oxide (rGO) material obtained from the reduction of a freeze-dried GO aerogel was used as an anode in the potassium-ion battery (PIB). Freeze-drying technique resulted in the preparation of porous rGO with high surface area ($219 \text{ m}^2/\text{g}$) and porous volume ($0.35 \text{ cm}^3/\text{g}$). Moving from linear to cyclic carbonate-based solvent electrolyte came with the decrease of the irreversible capacity at the first cycle, together with improved coulombic efficiency and cycle life. Very competitive performance of 267 mAh/g at C/3 rate with 78% capacity retention after 100 cycles were demonstrated. Electrochemical impedance spectroscopy (EIS) measurements evidenced the formation of a SEI layer at about 0.7 V vs. K^+ , followed by the reversible K-ion intercalation reaction at lower potential. The existence of a limited Warburg region in the EIS plot showed that the electrochemical process was mainly limited by the charge transfer process. The apparent diffusion coefficient of K ions was found to be about $10^{-9} \text{ cm}^2/\text{s}$ at 0.1 V vs. K^+ , which is higher compared to that measured with graphite electrodes, in agreement with the open porous structure of the freeze-dried rGO electrode which offers highly accessible surface.

Acknowledgements

The authors thank the French Agence Nationale de la Recherche (Labex STOREX programme) for funding of the research. LL thanks the China Scholarship Council for funding.

Conflict of Interest

The authors declare no conflict of interest.

Appendix A. Supporting information

References

- [1] H. Kim, J.C. Kim, M. Bianchini, D.-H. Seo, J. Rodriguez-Garcia, G. Ceder, Recent Progress and Perspective in Electrode Materials for K-Ion Batteries, *Adv. Energy Mater.* 8 (2018) 1702384.
- [2] C. Delmas, Sodium and Sodium-Ion Batteries: 50 Years of Research, *Adv. Energy Mater.* 8 (2018) 1703137.
- [3] C. Vaalma, D. Buchholz, M. Weil, S. Passerini, A cost and resource analysis of sodium-ion batteries, *Nat. Rev. Mater.* 3 (2018) 18013.
- [4] J. Mao, T. Zhou, Y. Zheng, H. Gao, H.K. Liu, Z. Guo, Two-dimensional nanostructures for sodium-ion battery anodes, *J. Mater. Chem. A.* 6 (2018) 3284–3303.
- [5] P. Barpanda, L. Lander, S. Nishimura, A. Yamada, Polyanionic Insertion Materials for Sodium-Ion Batteries, *Adv. Energy Mater.* 8 (2018) 1703055.
- [6] S. Chen, C. Wu, L. Shen, C. Zhu, Y. Huang, K. Xi, Challenges and Perspectives for NASICON-Type Electrode Materials for Advanced Sodium-Ion Batteries, 1700431 (2017) 1–21.
- [7] K. Saravanan, C.W. Mason, A. Rudola, K.H. Wong, P. Balaya, The First Report on Excellent Cycling Stability and Superior Rate Capability of $\text{Na}_3\text{V}_2(\text{PO}_4)_3$ for Sodium Ion Batteries, *Adv. Energy Mater.* 3 (2013) 444–450.
- [8] V.M. Kovrugin, J.-N. Chotard, F. Fauth, A. Jamali, R. David, C. Masquelier, Structural and electrochemical studies of novel $\text{Na}_7\text{V}_3\text{Al}(\text{P}_2\text{O}_7)_4(\text{PO}_4)$ and $\text{Na}_7\text{V}_2\text{Al}_2(\text{P}_2\text{O}_7)_4(\text{PO}_4)$ high-voltage cathode materials for Na-ion batteries, *J. Mater. Chem. A.* 5 (2017) 14365–14376.
- [9] V.M. Kovrugin, R. David, J.-N. Chotard, N. Recham, C. Masquelier, A High Voltage Cathode Material for Sodium Batteries: $\text{Na}_3\text{V}(\text{PO}_4)_2$, *Inorg. Chem.* 57 (2018) 8760–8768.
- [10] H. Pan, Y.S. Hu, L. Chen, Room-temperature stationary sodium-ion batteries for large-scale electric energy storage, *Energy Environ. Sci.* 6 (2013) 2338–2360.
- [11] S. Komaba, T. Hasegawa, M. Dahbi, K. Kubota, Potassium intercalation into graphite to realize high-voltage/high-power potassium-ion batteries and potassium-ion capacitors, *Electrochem. Commun.* 60 (2015) 172–175.
- [12] M. Okoshi, Y. Yamada, S. Komaba, A. Yamada, H. Nakai, Theoretical Analysis of Interactions between Potassium Ions and Organic Electrolyte Solvents: A Comparison with Lithium, Sodium, and Magnesium Ions, *J. Electrochem. Soc.* 164 (2017) A54–A60.
- [13] Y. Hamon, T. Brousse, F. Jousse, P. Topart, P. Buvat, D.M. Schleich, Aluminum negative electrode in lithium ion batteries, *J. Power Sources.* 97–98 (2001) 185–187.
- [14] Y. Mizutani, T. Abe, K. Ikeda, E. Ihara, M. Asano, T. Harada, M. Inaba, Z. Ogumi, Graphite intercalation compounds prepared in solutions of alkali metals in 2-methyltetrahydrofuran and 2, 5-dimethyltetrahydrofuran, *Carbon* N. Y. 35

- (1997) 61–65.
- [15] Z. Jian, W. Luo, X. Ji, Carbon Electrodes for K-Ion Batteries, *J. Am. Chem. Soc.* 137 (2015) 11566–11569.
- [16] X. Jiang, T. Zhang, L. Yang, G. Li, J.Y. Lee, A Fe/Mn-Based Prussian Blue Analogue as a K-Rich Cathode Material for Potassium-Ion Batteries, *ChemElectroChem.* 4 (2017) 2237–2242.
- [17] C. Zhang, Y. Xu, M. Zhou, L. Liang, H. Dong, M. Wu, Y. Yang, Y. Lei, Potassium Prussian Blue Nanoparticles: A Low-Cost Cathode Material for Potassium-Ion Batteries, *Adv. Funct. Mater.* 27 (2017) 1604307.
- [18] Z. Jian, S. Hwang, Z. Li, A.S. Hernandez, X. Wang, Z. Xing, D. Su, X. Ji, Hard–Soft Composite Carbon as a Long-Cycling and High-Rate Anode for Potassium-Ion Batteries, *Adv. Funct. Mater.* 27 (2017) 1–6.
- [19] X. Qi, K. Huang, X. Wu, W. Zhao, H. Wang, Q. Zhuang, Z. Ju, Novel fabrication of N-doped hierarchically porous carbon with exceptional potassium storage properties, *Carbon N. Y.* 131 (2018) 79–85.
- [20] I. Sultana, T. Ramireddy, M.M. Rahman, Y. Chen, A.M. Glushenkov, Tin-based composite anodes for potassium-ion batteries, *Chem. Commun.* 52 (2016) 9279–9282.
- [21] X. Ren, Q. Zhao, W.D. McCulloch, Y. Wu, MoS₂ as a long-life host material for potassium ion intercalation, *Nano Res.* 10 (2017) 1313–1321.
- [22] K. Xie, K. Yuan, X. Li, W. Lu, C. Shen, C. Liang, R. Vajtai, P. Ajayan, B. Wei, Superior Potassium Ion Storage via Vertical MoS₂ “Nano-Rose” with Expanded Interlayers on Graphene, *Small.* 13 (2017) 1–8.
- [23] W. Luo, J. Wan, B. Ozdemir, W. Bao, Y. Chen, J. Dai, H. Lin, Y. Xu, F. Gu, V. Barone, L. Hu, Potassium Ion Batteries with Graphitic Materials, *Nano Lett.* 15 (2015) 7671–7677.
- [24] Z. Ju, S. Zhang, Z. Xing, Q. Zhuang, Y. Qiang, Y. Qian, Direct Synthesis of Few-Layer F-Doped Graphene Foam and Its Lithium/Potassium Storage Properties, *ACS Appl. Mater. Interfaces.* 8 (2016) 20682–20690.
- [25] G. Ma, K. Huang, J.S. Ma, Z. Ju, Z. Xing, Q.C. Zhuang, Phosphorus and oxygen dual-doped graphene as superior anode material for room-temperature potassium-ion batteries, *J. Mater. Chem. A.* 5 (2017) 7854–7861.
- [26] Z. Ju, P. Li, G. Ma, Z. Xing, Q. Zhuang, Y. Qian, Few layer nitrogen-doped graphene with highly reversible potassium storage, *Energy Storage Mater.* 11 (2018) 38–46.
- [27] D. Cai, S. Wang, L. Ding, P. Lian, S. Zhang, F. Peng, H. Wang, Superior cycle stability of graphene nanosheets prepared by freeze-drying process as anodes for lithium-ion batteries, *J. Power Sources.* 254 (2014) 198–203.
- [28] A. Ponrouch, E. Marchante, M. Courty, J.M. Tarascon, M.R. Palacin, In search of an optimized electrolyte for Na-ion batteries, *Energy Environ. Sci.* 5 (2012) 8572–8583.

- [29] A. Ponrouch, R. Dedryvère, D. Monti, A.E. Demet, J.M. Ateba Mba, L. Croguennec, C. Masquelier, P. Johansson, M.R. Palacín, Towards high energy density sodium ion batteries through electrolyte optimization, *Energy Environ. Sci.* 6 (2013) 2361.
- [30] M. Dahbi, N. Yabuuchi, K. Kubota, K. Tokiwa, S. Komaba, Negative electrodes for Na-ion batteries, *Phys. Chem. Chem. Phys.* 16 (2014) 15007–15028.
- [31] J. Zhao, X. Zou, Y. Zhu, Y. Xu, C. Wang, Electrochemical Intercalation of Potassium into Graphite, *Adv. Funct. Mater.* 26 (2016) 8103–8110.
- [32] V. Augustyn, J. Come, M.A. Lowe, J.W. Kim, P.-L. Taberna, S.H. Tolbert, H.D. Abruña, P. Simon, B. Dunn, *Nat. Mater.* 12 (2013) 518–522.
- [1] S. Komaba, T. Hasegawa, M. Dahbi, K. Kubota, Potassium intercalation into graphite to realize high-voltage/high-power potassium-ion batteries and potassium-ion capacitors, *Electrochem. Commun.* 60 (2015) 172–175.
- [2] Y. Hamon, T. Brousse, F. Jousse, P. Topart, P. Buvat, D.M. Schleich, Aluminum negative electrode in lithium ion batteries, *J. Power Sources.* 97–98 (2001) 185–187.
- [3] M. Okoshi, Y. Yamada, S. Komaba, A. Yamada, H. Nakai, Theoretical Analysis of Interactions between Potassium Ions and Organic Electrolyte Solvents: A Comparison with Lithium, Sodium, and Magnesium Ions, *J. Electrochem. Soc.* 164 (2017) A54–A60.